

# MultiSAS, a six degrees of freedom vibration isolation system for Advanced Virgo

J.V. van Heijningen<sup>1,2,a,†</sup>, A. Bertolini<sup>1</sup>, E. Hennes<sup>1</sup>,  
M.G. Beker<sup>1,2,b</sup>, M. Doets<sup>1</sup>, H.J. Bulten<sup>1,2</sup>, K. Agatsuma<sup>1,c</sup>,  
T. Sekiguchi<sup>d</sup> and J.F.J. van den Brand<sup>1,2</sup>

<sup>1</sup>National Institute for Subatomic Physics Nikhef, Science Park 105, 1098 XG Amsterdam, The Netherlands

<sup>2</sup>VU University, De Boelelaan 1105, 1081 HV Amsterdam, The Netherlands

<sup>a</sup>present affiliation: OzGrav-UWA node, University of Western Australia, 35 Stirling Hwy, Crawley WA 6009, Australia

<sup>b</sup>present affiliation: Innoseis B.V., Science Park 105, 1098 XG Amsterdam, The Netherlands

<sup>c</sup>present affiliation: The University of Birmingham, Edgbaston, Birmingham B15 2TT, United Kingdom

<sup>d</sup>present affiliation: Halley Valley Co. Ltd., Taiyo-Life Shinagawa Building 28F, 2-16-2 Konan, Minato-ku, Tokyo 108-0075, Japan

E-mail: [†joris.vanheijningen@uwa.edu.au](mailto:†joris.vanheijningen@uwa.edu.au)

August 2018

**Abstract.** We present a compact, vacuum compatible seismic attenuation system designed to isolate five auxiliary optical benches for Advanced Virgo, a second generation gravitational wave detector. We report on the design of the device, coined MultiSAS (Multistage Seismic Attenuation System) and on its measured vibration isolation performance. The latter can be summarized by quoting a payload isolation ratio at 10 Hz of 100 dB and 140 dB in vertical on horizontal, respectively. We also present the design and performance of the MultiSAS control system along the translation degrees of freedom, as well as a discussion of the possible coupling to the angular degrees of freedom. Over a timescale of 100 seconds, 1  $\mu\text{m}$  magnitude rms for translational degrees of freedom is achieved for all seismic conditions. The spectral displacement levels are expected to be lower than  $10^{-14}$  m/ $\sqrt{\text{Hz}}$  from 10 Hz onwards in vertical and horizontal. In addition we discuss effects that could deteriorate the performance of the device such as thermal drifts of the mechanical filters, residual acoustic coupling and so-called cradle effects on the inverted pendulum pre-isolation stage. Mitigation strategies or solutions were devised and installed in the five Advanced Virgo systems.

*Keywords:* Gravitational Waves, Vibration isolation, Seismic Noise, Controls

## 1. Introduction

With the detection of gravitational waves (GWs) [1], mankind has made its most precise distance measurement to date. After Advanced Virgo [2] joined the global GW detector network, the first triple-coincident measurement of GWs measured by Advanced Virgo and the two LIGO detectors [3], GW170814, was made in August 2017 [4]. Three days after Advanced Virgo's first detection, the first coincidental measurement of GWs with electromagnetic counterparts, GW170817, from a binary neutron star merger [5, 6] have provided a firm basis for the newly founded field of (multi-messenger) gravitational wave astronomy.

The detections would not have been achievable without the vibration isolation of all components of the gravitational wave detectors. In line with the earlier vibration isolation strategy of Initial Virgo [7], all new seismic attenuation systems for auxiliary optical benches for Advanced Virgo, called MultiSAS (Multistage Seismic Attenuation Stage) achieve their (in-band) performance through passive isolation by suspension of the optical benches. Active feedback is only used to control the low-frequency rigid body modes of the isolation chain. In total five are part of Advanced Virgo. In particular, the photodiodes responsible for measuring the GW signal of GW170814 and GW170817 are positioned on an optical bench, which is decoupled from Earth's motion the by MultiSAS unit.

Benches housing auxiliary optics generating error signals in order to control the interferometer are now suspended and in vacuum. The decision of suspending the benches in vacuum was made to limit the vibrations of the optical sensors themselves that can couple to the alignment control signals [8]. Another reason to mitigate the noise caused by the light scattered back towards the interferometer by the control photodiodes and their telescopes optics. This light is modulated by the residual seismic motion of the bench. The non-linear behavior of this coupling leads to the upconversion of low-frequency seismic excitations ( $< 10$  Hz) into the detection band ( $> 10$  Hz) [9, 10]. This was a serious limitation on the achievable sensitivity of first generation detectors. Any bench motion will be indistinguishable from a beam displacement on the suspended auxiliary optics due to a misalignment of the cavity mirrors. Hence the real bench displacement noise should not exceed the optical sensor shot noise contribution to the measurement.

In Section 2 we summarize the extensive characterization campaign of the MultiSAS prototype, including an overview of lessons learned and improvements implemented in the final design of the five Advanced Virgo systems. The results and performance of the MultiSAS prototype are presented in section 3. In Section 4, various performance deteriorating issues and their solution/mitigation strategies are discussed. The mechanical modes of the system are sensed and controlled and the control performance is presented in Section 5. Finally, we make concluding remarks and discuss future work towards next generation gravitational wave detectors.

## 2. MultiSAS Design

MultiSAS is designed to comply with rms requirements as well as a amplitude spectral density (ASD) requirements for the optical bench motion at 10 Hz by using chains of low natural frequency ( $f_0 < 1$  Hz) mechanical filters. The seismic attenuation system  
 45 isolates the suspended object from seismic motion. Typically the microseismic peak provides the largest contribution to the integrated motion of the ground [13]. This peak is roughly between 200 and 500 mHz at the Virgo site. A summary of the requirements is given in Table 1.

**Table 1.** Requirements [8] for translational and angular motion of the optical benches suspended by MultiSAS.

	translational ( $z$ )	angular ( $\theta_z$ )
Integrated rms (down to 10 mHz)	$1 \times 10^{-6}$ m	$3.1 \times 10^{-8}$ rad
ASD from 10 Hz onwards	$2.1 \times 10^{-12}$ m/ $\sqrt{\text{Hz}}$	$3.3 \times 10^{-15}$ rad/ $\sqrt{\text{Hz}}$

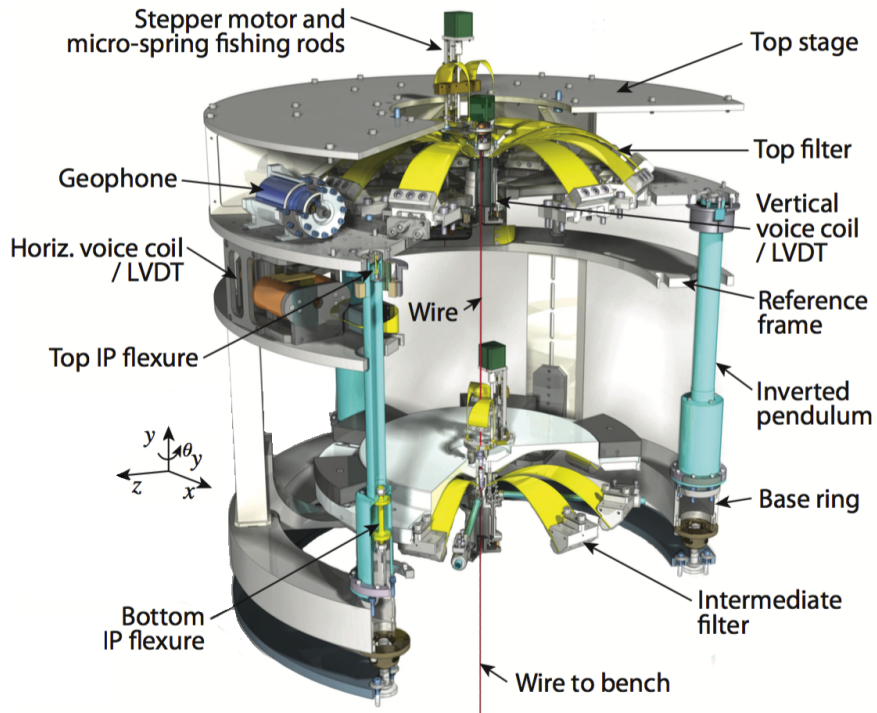


**Figure 1.** Mechanical overview of the MultiSAS isolation system. The position of sensors and actuators are visible in the structure. Bench translational control uses sensors and actuators at the top stage. Vertical control is done only with the top filter LVDT [12]/ voice coil pair. The top and intermediate filters have stepper motors with springs for vertical positioning. The Virgo coordinate system is displayed, which has the  $z$ -direction along the beam and the  $y$ -direction as vertical. This coordinate system will be used through this article.

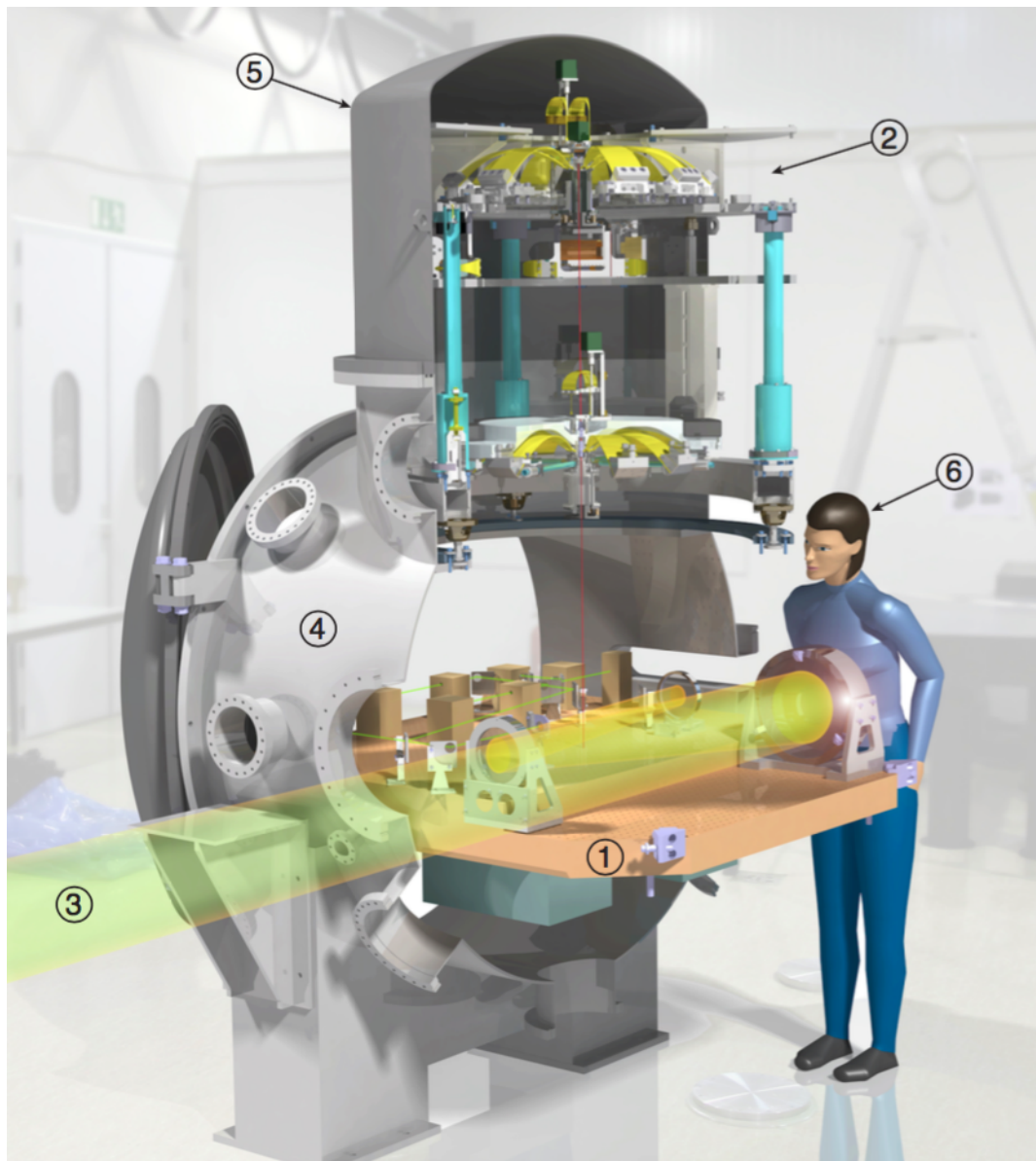


**Figure 2.** An impression of MultiSAS suspending an Advanced Virgo optical (end) bench in a MiniTower vacuum chamber. 1) Optical bench. 2) MultiSAS. 3) Transmission beam from end mirror. 4) MiniTower vacuum chamber. 5) Removable cupola. 6) Observant physicist.

The mechanical filters are a chain of (inverted) pendulums for horizontal isolation and a chain of Geometric Anti-Spring (GAS) [15] filters. Fig. 1 shows the complete  
50 mechanical design of MultiSAS: a compact, vacuum compatible and high performance vibration isolation system. From the base ring, an inverted pendulum stage supports the top filter structure. From the first GAS filter stage, a wire suspends the intermediate filter. The intermediate filter body holds a second set of GAS blade springs, which  
55 suspends the optical bench via another wire. The two wires act as pendulums provides two more stages of horizontal isolation.

As shown in Fig. 1, the fishing rod is a set of maraging steel springs which base moves vertically on a stepper motor. This results in a variable DC pulling force that can be altered when *e.g.* a temperature change alters the vertical position of the GAS filters. In a GAS filter the blades are held in place by clamps on the outside, while their tips are connected to a single keystone from which the intermediate stage or payload is suspended. This keystone is designed to move in the vertical degree of freedom and be geometrically stiff in all other degrees of freedom. High frequency ( $> 50$  Hz) modes in translational and angular keystone modes exist and these are discussed at the end of next section.

A set of sensors and actuators is used to effectively damp the rigid body modes of (inverted) pendulum and GAS filters, without spoiling the passive isolation performance. The isolation structure of Fig. 1 fits in one cubic meter to be compliant with the limited space available in the existing Virgo infrastructure. Each system is placed in a vacuum vessel coined MiniTower and the base ring rests on an appropriate support inside this vacuum vessel, as is shown in Fig. 2.

### 3. Isolation Performance

The individual stages of the total system, *e.g.* the inverted pendulum stage and the GAS filter chains, were tested. The transfer function of the inverted pendulum stage was determined by a measurement at Nikhef [17], where the stage was loaded by a single pendulum dummy mass. After tuning the counterweights on the legs, the transfer function follows the ideal  $1/f^2$  slope up to about 20 Hz with an achieved isolation below  $2 \times 10^{-4}$  from 20 Hz onwards. The primary motivation for the measurement was to tune the center of percussion effect [16] by adjusting the counterweights at the bottom of the inverted pendulum legs.

The inverted pendulum stage was put on three piezo shaker stages (indicated by red arrows) to measure the horizontal transfer function as shown in Fig. 3. In order to measure a transfer function, horizontal accelerometers were placed on the base ring as well as the top stage. Much effort was put in tuning the center of percussion effect by adding or removing mass from the so-called counterweight holding bell located at the bottom of the inverted pendulum legs. It was determined that five blocks of 140 g, totaling at 700 g per inverted pendulum leg, gave the best results. The final result is shown in Fig. 4.

In the earliest stages of the prototype tests [14], the main performance of the inverted pendulum and the GAS filter chains have been characterized. The GAS blades are fabricated out of maraging steel, a low creep, high strength material. The local transfer function from the base ring to the bench suspension point is obtained by combining the transfer functions discussed earlier to obtain the MultiSAS overall transfer functions. It features isolation ratios of  $10^5$  and  $10^7$  for vertical and horizontal motion, respectively, at 10 Hz as is presented in Fig. 5.

The vertical and horizontal transfer function have a slope of  $1/f^4$  and  $1/f^6$ ,

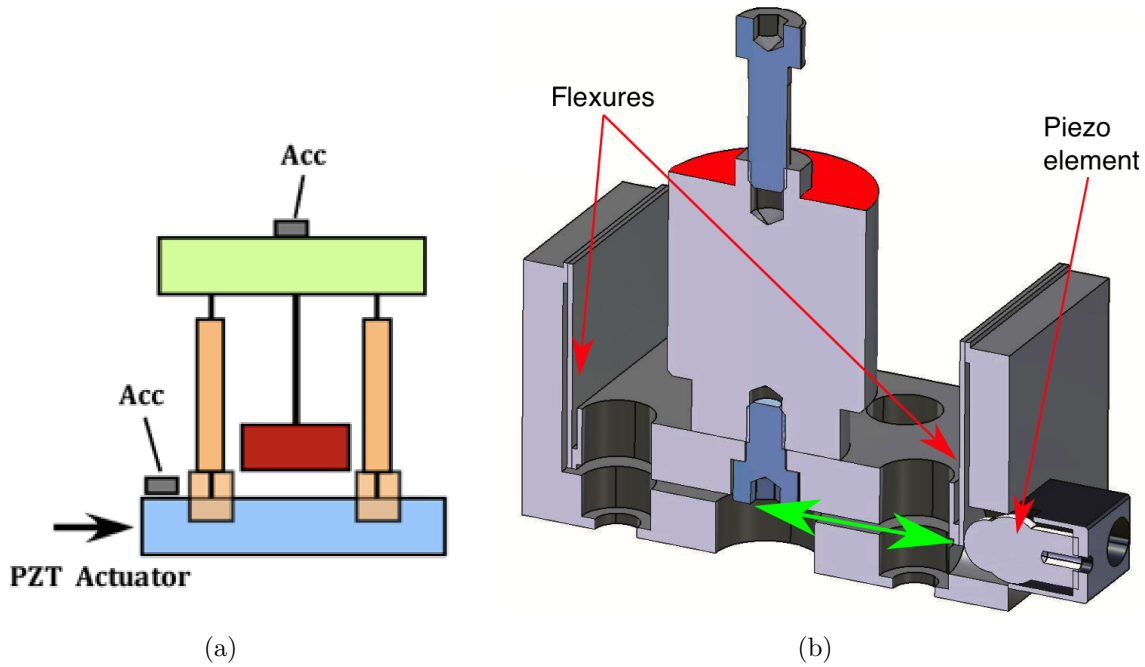


**Figure 3.** Panel (a) shows a cartoon of the set-up for the inverted pendulum stage transfer function measurement. Horizontal accelerometers are used to record the transfer. To avoid exciting the reference frame modes, the reference frame was detached and lifted from the base ring. Tilt coupling to the top stage accelerometer proved to be a problem and much effort was put in positioning it to mitigate these issues. Panel (b) shows a CAD drawing of a piezo shaker. The base ring rests on three custom made horizontal flexure stages driven by piezo actuators. The green arrow indicates the direction of motion.

respectively, up to about 30 Hz. For the horizontal isolation, the inverted pendulum mode tuned down to 100 mHz or lower; the pendulum modes (of the intermediate mass and bench double pendulum system) are around 0.7 Hz and 1.8 Hz for the Advanced Virgo design wire lengths and overall mass distribution. GAS filters are typically tuned such that the cascade of two GAS filters in MultiSAS results in modes around 200 and 600 mHz.

At the Virgo site, the typical seismic motion at 10 Hz is below  $10^{-9}$  m/ $\sqrt{\text{Hz}}$ . The isolation performance of  $10^7$  in horizontal motion is sufficient by (more than) two orders of magnitude in order to meet the requirement of  $2.1 \times 10^{-12}$  m/ $\sqrt{\text{Hz}}$  at 10 Hz. There is a residual horizontal-to-angular coupling due to the bench center of mass does not coinciding with its suspension point. A horizontal motion will couple to a pitch and roll motion of the bench. Yaw coupling is difficult to model and the residual angular motion at 10 Hz is not deemed a problem as for the optical benches the mode is expected to be about 20 mHz.

The equation of motion for the pitch or roll degree of freedom (denoted  $\theta_z$  in the following discussion) for the bench is

$$I_{\text{cm},x} \ddot{\theta}_z + k_{\theta_z} \theta_z = d_{\text{susp}} \cdot m_b \ddot{x}, \quad (1)$$

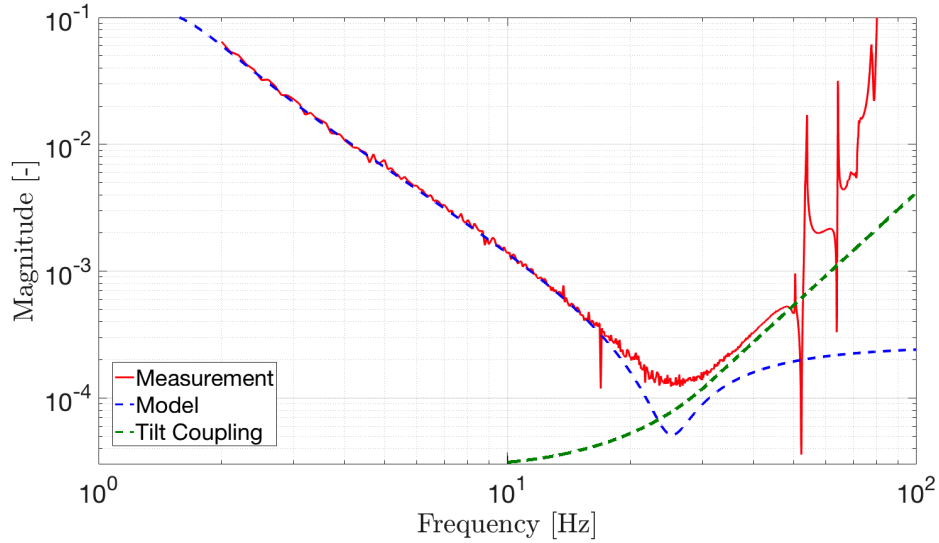


**Figure 4.** Inverted pendulum transfer function measurement result. The center of percussion effect is modeled to be slightly overcompensated with a  $Q=5$  resonant zero at 25 Hz. The saturation level is almost 80 dB. Residual tilt coupling of the measurement set-up is visible from 25 Hz onwards. This is a roll-up of a tilt resonance of the piezo suspension shown in Fig. 3(b) and a measurement artifact. Several internal modes of the shaker stage are visible above 50 Hz.

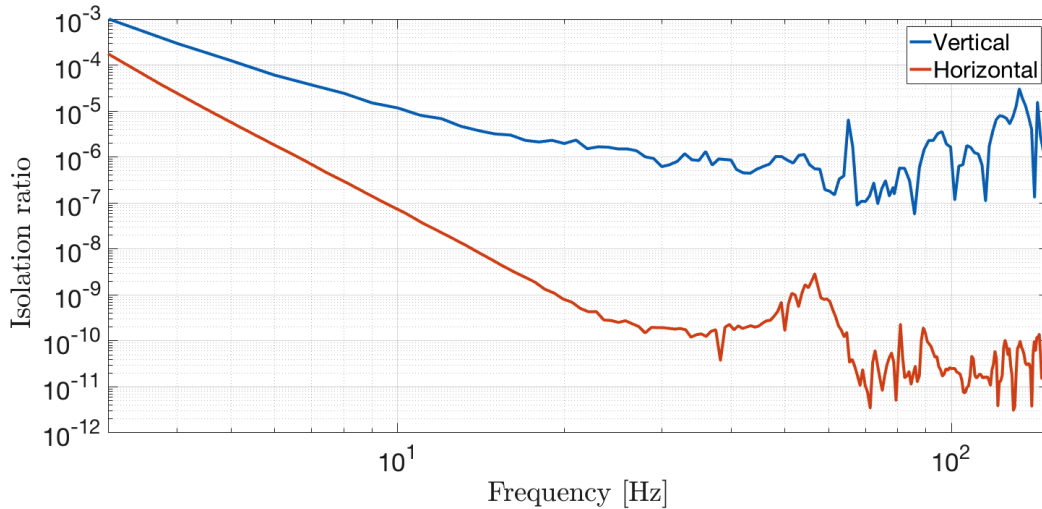


**Figure 5.** Reconstructed vertical [14] and horizontal transfer functions of MultiSAS. Both results are obtained by multiplying intermediate transfer functions, e.g. from actuator structure to top stage to characterize the inverted pendulum stage. The structures from 65 Hz onwards in vertical are resonances of modes of the system, where the first higher order vertical mode at 135 Hz is associated with an intermediate filter keystone bouncing mode. The structure from 40 Hz onwards in horizontal are the (damped) keystone modes described above.

where  $I_{\text{cm},z}$  represents the moment of inertia around the  $z$  axis,  $k_{\theta_z}$  the angular stiffness at the suspension rotation point,  $m_b$  the mass of the bench and  $d_{\text{susp}}$  the distance

between the suspension rotation point and the bench center of mass. Modelling the bench as a homogeneous, rectangular box yields

$$I_{\text{cm},z} = \frac{1}{12}m_{\text{b}}(h_{\text{b}}^2 + l_{\text{b}}^2), \quad (2)$$

where  $h_{\text{b}}$  and  $l_{\text{b}}$  represent the height and length of the bench, respectively. A more precise  $I_{\text{cm}}$  can be obtained from a CAD model of the suspended object. This can deviate by a factor of two or more depending on the mass distribution of the suspended object.

Taking the Laplace transform of Eq. (1) results in

$$\tilde{\theta}_z = \frac{12d_{\text{susp}}}{(h_{\text{b}}^2 + l_{\text{b}}^2) \left(1 - \frac{12}{h_{\text{b}}^2 + l_{\text{b}}^2} \frac{\omega_{0,\theta_x}}{\omega}\right)} \tilde{X}, \quad (3)$$

where  $\omega_{0,\theta_x}$  is the pitch or roll resonance frequency. For high frequencies Eq. (3) reduces to

$$\tilde{\theta}_z \approx \frac{12d_{\text{susp}}}{(h_{\text{b}}^2 + l_{\text{b}}^2)} \tilde{X}. \quad (4)$$

The populated bench geometry is such that this coupling can easily exceed 0.1 rad/m, so that is why the horizontal isolation performance of MultiSAS has to be sufficient also to meet the angular requirement of  $3.3 \times 10^{-15}$  rad/ $\sqrt{\text{Hz}}$  at 10 Hz. In other words, the angular requirement dictates the translational requirement.

After MultiSAS was installed into a MiniTower further characterization was performed on the full mechanical assembly. Unwanted in-band ( $> 10$  Hz) resonances were identified by hammering tests and transfer function measurements and studied by Finite Element Modeling (FEM). Fig. 6 and Fig. 7 show two important ones and our solutions to damp them.

The combined lateral and rotational modes of the keystone show up as large peaks in the transfer function. By placing a circular slab of steel on three pieces of viton on the keystone, its resonances are successfully damped, as shown in Fig. 6(b).

The bench is suspended from the intermediate filter by a two part wire with a steel connection joint, shown in Fig. 7(a). This joint is used to trim the vertical position of the bench. Its lateral swing modes show up as a large peak at 75 Hz in the transfer from the intermediate filter to the bench. Fortunately, electrical power and signal cables, carefully routed via an aluminium support plate attached to the wire (see Fig. 7(b)) to the bench to maintain isolation performance, have a profound effect on this mode. The mass of this holder is pushing the mode frequency down to about 55 Hz and helps to damp the peak.

#### 4. Thermal Shielding, Acoustic Coupling and Leg Parallelism Measurement

Several aspects that could be detrimental to the seismic isolator performance have been characterized and mitigation strategies have been devised. Three of these possible

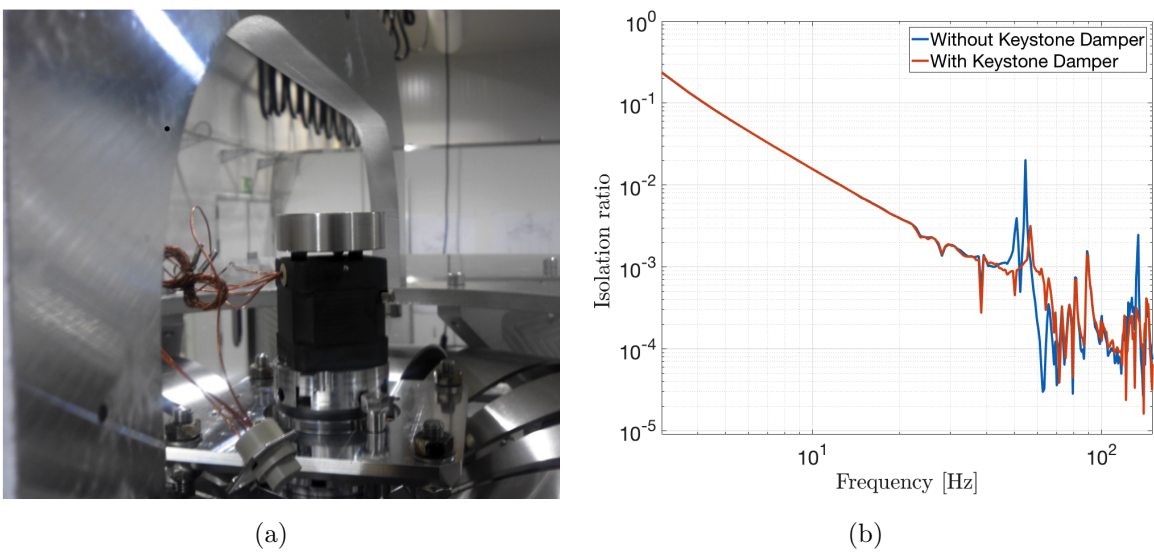


**Figure 6.** Effect of a damper on the MultiSAS Topstage GAS filter keystone: (a) a photograph of the damper on the keystone and (b) a comparison in horizontal isolation ratio from top stage to intermediate filter without and with such a damper. The keystone resonances are the peaks at 55 Hz and 125 Hz. Other structures found at 80 Hz, between 75 Hz and 100 Hz and between 140 Hz and 150 Hz are the resonance of the filter frame, coupling with the actuator support structure and the top filter GAS blades resonances, respectively.

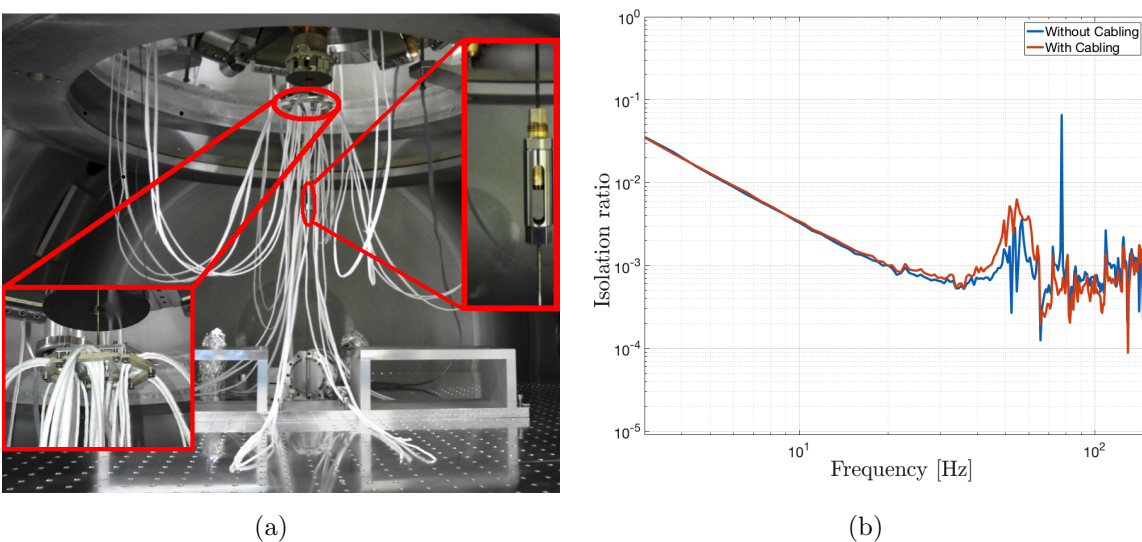


**Figure 7.** Panel (a) shows a photograph of the area between intermediate filter to the bench. The right and left insets are zooms of the wire connector and the cable support plate, respectively. Panel (b) shows the horizontal transfer from intermediate filter to bench without and with cabling.

issues, *i.e.* thermal effects on the GAS filters, acoustic couplings and the so-called cradle effect, and their solution or mitigation are presented here.

In all suspended benches the front-end and digital processing electronics for the

hosted photodetectors are housed in an air-tight container which is a structural part of the bench itself. In this way, most of the cabling, that could act as a short for seismic noise, has been eliminated. All digital in/out signals are carried by highly compliant optical fibers, and the only cable routed throughout the bench suspension is the power supply one. The most temperature sensitive elements of MultiSAS are (the blades of) the two GAS filters. The thermo-elasticity of maraging steel causes a change of -250 ppm/K in the loading capability corresponding to -1.05 N/K for the top stage GAS filter (nominal load of 430 kg for a typical Advanced Virgo suspended bench) and -0.78 N/K for the intermediate stage GAS filter (nominal load of 320 kg). The result is a vertical position drift

$$\Delta y = \frac{g}{\omega_0^2} \frac{\Delta E}{E}, \quad (5)$$

where  $E$  represents the Young's modulus and  $\omega_0$  the filter's resonance frequency. Less dominant is the detuning of the filter due to the differential thermal expansion coefficient between maraging steel and the filter body material, which alters the blade compression rate slightly. The filter body material is stainless steel for both top and intermediate filter. This detunes the filter, *i.e.* causes a change in the resonance frequency by tens of mHz.

Continuous compensation for the position drift  $\Delta y$  during operation of the sensing optics on the bench is provided by the top stage GAS filter built-in voice coil actuator. This actuator has a dynamic range of  $\pm 1.5$  N. Long term drift compensation can be made by using the fishing rod actuators installed on both the filters and with a dynamic range from 3.3 N to 9.3 N. MultiSAS can operate with a maximum thermal drift of 7.5 K<sub>pp</sub> from initial set point.

Since the benches are expected to operate in vacuum at a temperature around 40° Celsius, a thermal shield was designed and its efficiency tested on the MultiSAS prototype [18]. The thermal shield consists of a stack of two closely spaced (about 10 cm) non-anodized reflective aluminum sheets attached to the MultiSAS base ring. An anodized black aluminum plate to simulate the radiating surface of the warm optical bench equipped with resistive heaters was secured on top of the suspended bench. This set-up with the position of two thermal shields below the intermediate filter.

In Fig. 8, the heat shields are tested when both shields are reflective. Prior to that, a test was performed with the bottom shield anodized black. Especially the shields and also the filter blades were warmer when the temperature settled. The tests are performed under vacuum, as visible in Fig 8(a) in the first hour. The buoyancy effect of the bench not floating in a bath of air anymore increases the load slightly for the MultiSAS and causes a sag. The increasing temperature of the filter blades makes the keystones sag. Over a day bench has sagged by almost 2 mm and longer tests have shown that this process continues. The bench can end up 4 mm below its starting point, but is within the range of the 2 fishing rods on the top and intermediate filter stage. In Fig 8(b) we observe that, while the *hot plate* (a resistive plate installed just above the bench to simulate radiating electronics) heats up to about 45° C, the top stage and intermediate

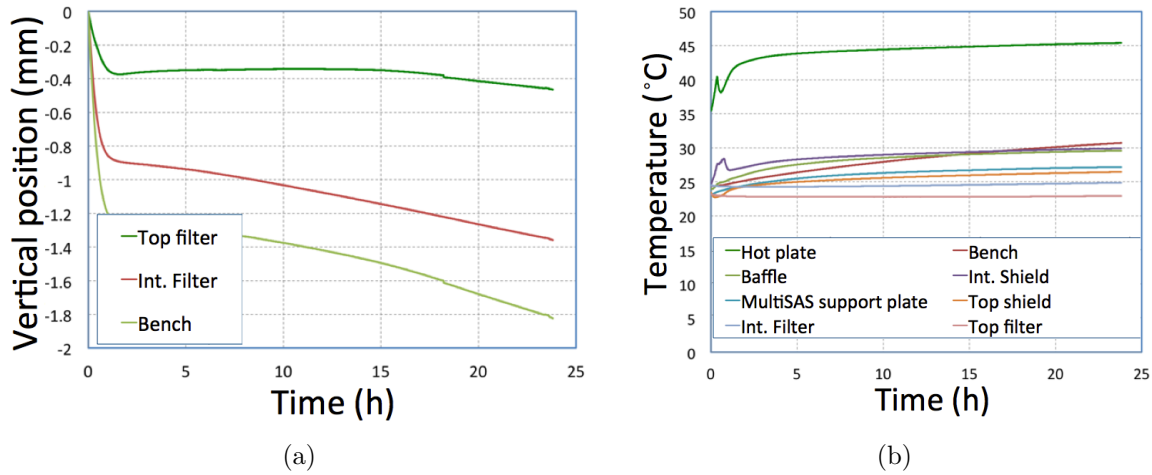


**Figure 8.** Thermal shield equilibrium performance showing (a) the GAS filter keystone and bench position. The small jump down around 18h into the test is attributed to hysteresis in the top stage blades. Panel (b) shows MiniTower and MultiSAS temperatures during this measurement.

195 stage blades reach temperatures of 23° C and 25° C, respectively.

Operating a suspension in air has certain limitations at in-band ( $f > 10$  Hz) frequencies. Acoustic pressure waves push on the otherwise isolated suspended object, such as an optical table. Removing the air eliminates the medium these pressure waves use to travel through and reduces the so-called acoustic coupling. The optical benches that are suspended by MultiSAS for Advanced Virgo are all in their MiniTower, where a vacuum of better than  $10^{-4}$  mbar can be achieved. A scroll pump can bring the pressure below 1 mbar and a turbo pump can bring the pressure down even further.

200 A dedicated test to investigate how the bench ambient pressure relates to the acoustic coupling, a test was performed. Six inertial sensors, Sercel L22 geophones, were installed on the bench. With these six geophones (three horizontal and three vertical), the bench motion in all degrees of freedom can be reconstructed and the impact of acoustic noise can be evaluated. The limit of the measurement is set by the self noise of the geophones. The self noise of the L22 geophone at 10 Hz is about  $2 \times 10^{-12}$  m/ $\sqrt{\text{Hz}}$  and falls off with  $1/f$  from that point.

210 For the test the vacuum vessel is vented to a pressure of 10 mbar. The scroll pump continues to pump and the pressure is monitored. When the pressure is below 1 mbar, the turbo pump takes over and reduces to pressure to below  $10^{-4}$  mbar over an hour. The horizontal coupling effect is displayed in Fig. 9. Below 5 mbar the acoustic coupling drops below the L22 self-noise. This indicates that, to maintain the translational isolation performance of MultiSAS, it must be operated at a pressure of 5 mbar or below. For the angular motion, for which a horizontal motion at the  $10^{-15}$  m/ $\sqrt{\text{Hz}}$  is desirable, this measurement can give an upper limit.

215 Because of tolerances in machining and assembly, MultiSAS inverted pendulum legs might not be perfectly parallel. Additionally, there might be a mismatch in leg length,

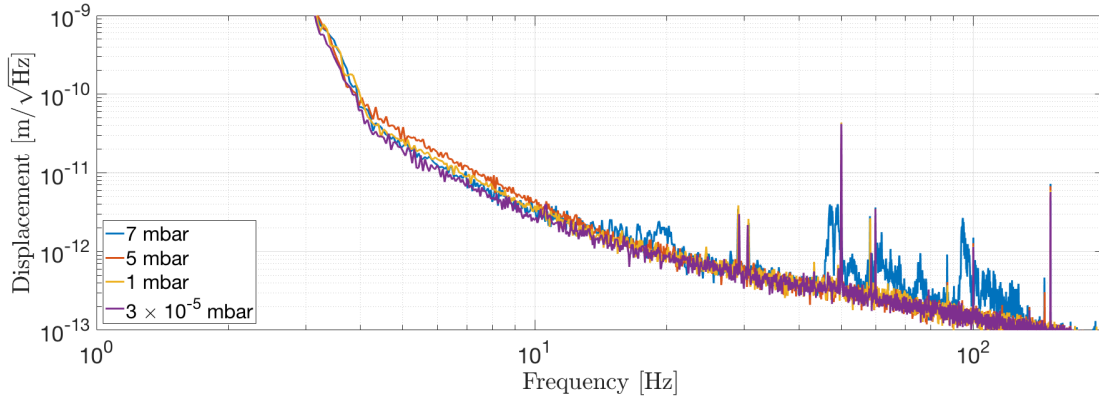


**Figure 9.** Acoustic coupling at a translationally and angularly controlled MultiSAS test facility suspended bench at different pressures for a horizontal L22 (out-of-loop) geophone on the bench. Clearly, the acoustic coupling falls below the L22 self noise below 5 mbar.

220 causing similar effects as described in this section. In Fig. ?? a perfect stage is shown  
 in the left picture, where lateral displacements do not result in the introduction of tilt  
 to the top plate. The middle and right picture illustrate the possible non-parallel leg  
 assembly. This is referred to as the cradle effect. This effect is highly exaggerated, but  
 the two distinct cases can be distinguished when looking at the phase of the signals with  
 225 respect to each other. The middle picture shows in-phase transfer from the  $x$  degree of  
 freedom to  $\theta_z$ , whereas the right picture shows a  $180^\circ$  out-of-phase transfer.

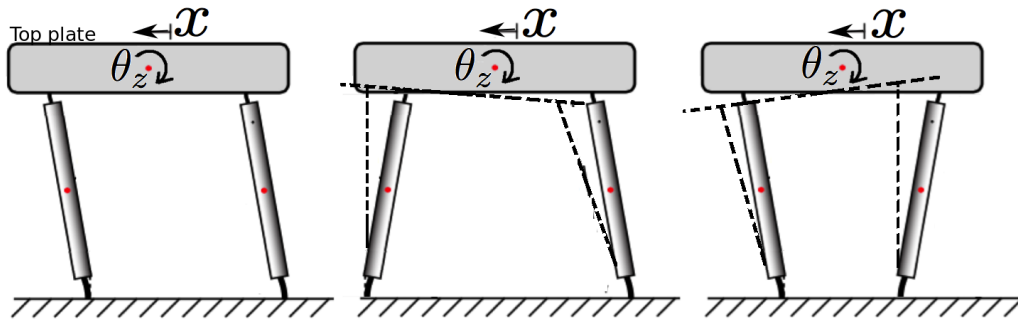


**Figure 10.** An overview of different possible cradle effects in the case of real world misalignments in leg-to-top-plate connections due to construction tolerances.

The parasitic coupling from displacement to tilt in the top stage cannot exceed a  
 certain value. This is because of the well known problem that inertial sensors (geophones  
 in our case) cannot distinguish between translation and tilt. Tests were performed both  
 230 on the prototype to measure the coupling coefficient, *i.e.* the misalignment between  
 the inverted pendulum legs. The tilt meter that was used is an Applied Geomechanics  
 755-1129 Miniature Tilt Sensor. The sensor has a  $100 \text{ nrad} / \sqrt{\text{Hz}}$  resolution [19]. The  
 measurement injected large 2 mm peak-peak, 5 mHz sinusoids in both horizontal  $x$  and  
 $z$  degrees of freedom. The injection is done at such a low frequency to be sure not to

excite any mode of the suspension system, *i.e.* the lowest resonance frequency.

Table 2 shows the results of the two, several hour long injections, where immediately it can be seen that all couplings are below the  $3 \times 10^{-3}$  rad/m level. The geophone measurement of the top stage displacement can be used down to the bandwidth lower frequency  $f_{LB} = 1/(2\pi)\sqrt{g c_{hta}}$ , where  $c_{hta}$  is the coupling from a horizontal to an angular degree of freedom. This means, in order to have an inertial sensor correctly measuring the displacement down to frequencies where the sensor self-noise becomes dominant, the coupling should not exceed the  $4 \times 10^{-2}$  rad/m level. The results of the measurements show that the typical leg misalignment is on the safe side by more than one order of magnitude. Measurements done on one of the MultiSASs for Advanced Virgo showed couplings all below the  $3 \times 10^{-3}$  rad/m level [20].

**Table 2.** Measured coupling factor  $c_{hta}$  from horizontal to angular displacement for the top stage of the MultiSAS prototype. All couplings are more than one order of magnitude smaller than the maximum allowed value in order to have the geophones measure displacement instead of tilt down to 100 mHz.

	$x \rightarrow \theta_x$	$x \rightarrow \theta_z$	$z \rightarrow \theta_x$	$z \rightarrow \theta_z$
$c_{hta}$	$8 \times 10^{-4}$	$1.5 \times 10^{-3}$	$7 \times 10^{-4}$	$2 \times 10^{-3}$ rad/m

## 5. Control Design and Performance

To maintain MultiSAS at its operating point and provide optimal performance, active feedback is implemented. The error signals used for this control scheme are constructed from three LVDTs, three Sercel L4C geophones placed on the top stage and, optionally, a tri-axial measurement of the ground motion. The LVDT is a differential DC sensor measuring the top stage position with respect to the reference frame which is connected to the MiniTower vacuum vessel. The L4C geophone is an inertial sensor. The signals from LVDTs and geophones are combined in the frequency domain (blended) to construct an inertial broadband super sensor with DC positioning. A cross-over frequency is chosen in this blend; below this frequency, the LVDT signal is used and the geophone signal is dominant above this cross-over frequency. Blending is done preferably below the microseismic peak, which is typically between 100 to 500 mHz [13], so that the L4C inertial signal is dominant in the blended signal at those frequencies. The microseismic peak can then be suppressed and the bench rms motion can be reduced.

As the ground is in the LVDT signal with opposite sign, the ground measurement can be added to the LVDT signal. This process is called ground subtraction. At the Nikhef set-up, a Trillium T240 seismometer measures the ground motion in three axes, *i.e.* the  $x$ -,  $y$ - and  $z$ -direction. The vertical motion is only sensed by a single LVDT within the keystone of the top GAS filter. Ground motion subtraction is vital for this degree of freedom. The use of low frequency blending makes the ground subtraction in horizontal less crucial.

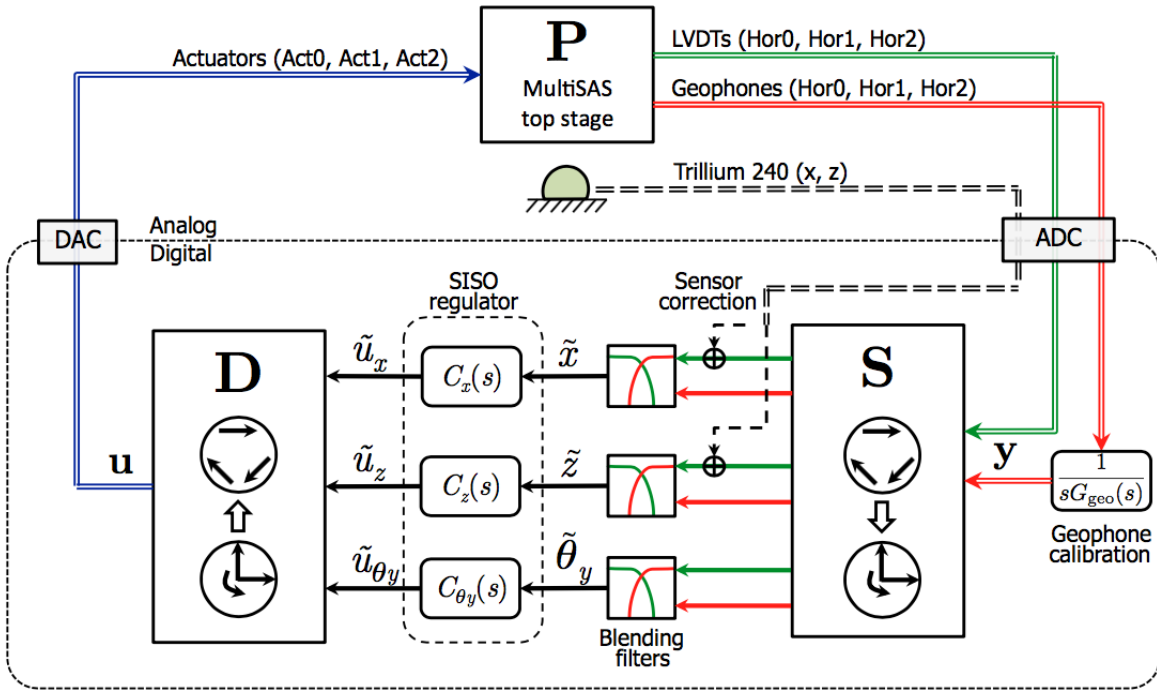


**Figure 11.** Horizontal digital control strategy for MultiSAS. A multitude of sensor signals is geometrically added (using matrix  $S$ ), blended to reconstruct virtual supersensors ( $x$ ,  $z$ ,  $\theta_y$ ) and implement single-input-single-output (SISO) control in those degrees of freedom. Control signals for virtual actuators are subsequently sent to each actuator by multiplying by matrix  $D$ . Reproduced from Ref. [14]

Fig 11 shows the horizontal control strategy for MultiSAS in Virgo. The control scheme features a fully digital control, using eight sensor inputs. These are blended to construct a DC coupled inertial for three horizontal degrees of freedom. Before  
 270 blending, the signals are geometrically added using the sensing matrix  $S$ . This matrix is determined by extraction of the different degrees of freedom ( $x$ ,  $z$  and  $\theta_y$ ) from the geometric content of each sensor signal.

The three horizontal error signals are sent to a SISO controller as per Fig 11. The controller response is shown in Fig. 12 with its zeros and poles presented in Table 3.

**Table 3.** Values for  $f$  and  $Q$  of the zeros and poles that make up the horizontal PID controller with elliptic roll-off filter. The real pole at 0 Hz represents the integrator. The gain is 35 at 1 Hz. The other top stage filters differ by the position of the  $Q = 0.5$  zero, which is  $f = 0.1$  Hz for  $\theta_y$  and  $y$  filters. The other difference is that the gain is 1.5 and 4 at 1 Hz for  $\theta_y$  and  $y$  filters, respectively.

Zeros		Poles	
$f$ [Hz]	$Q$	$f$ [Hz]	$Q$
0.07	0.5	0	-
25	50	4.58	0.88
		30	0.5

Visible in the plant transfer function are the main translational modes of MultiSAS (blue and red curves in Fig. 12). The inverted pendulum stage has a resonance frequency of about 100 mHz. From the top stage the intermediate filter and suspended bench act as a double pendulum. The common pendulum mode in anti-phase with the top stage is located around 0.7 Hz. This mode in phase with the top stage generates the notch around 0.4 Hz. The differential pendulum mode, where the intermediate filter and bench (and top stage) move out of phase, is located around 1.8 Hz. The top stage and intermediate phase in phase result in the notch around 1.6 Hz.

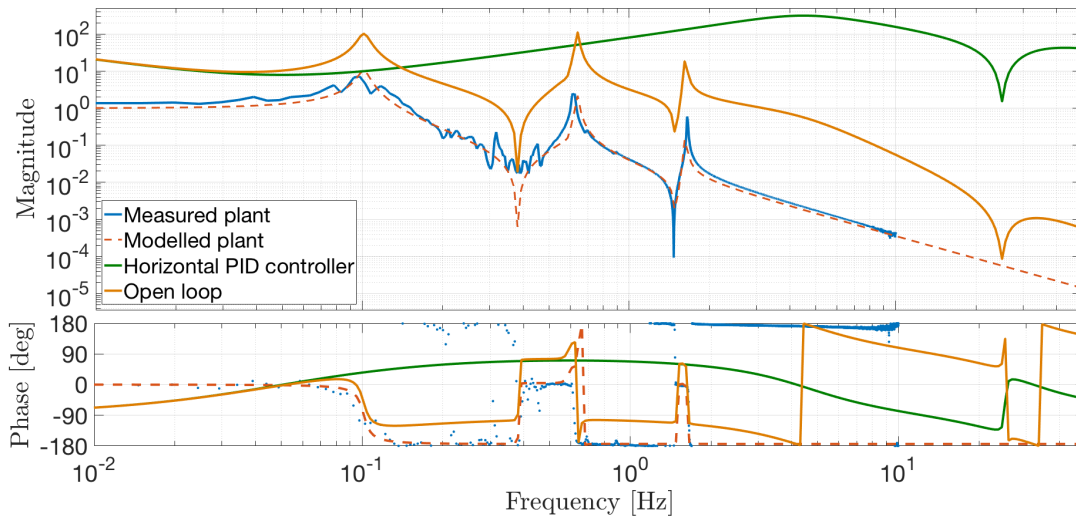


**Figure 12.** Loop transfer function design for the top stage MultiSAS horizontal degrees of freedom ( $x$ ,  $z$ ). A forced transfer function measurement of MultiSAS compared to the modelled transfer function. The control filter is a conventional PID filter with a steep roll off provided by a 1<sup>st</sup> order elliptic filter with a notch at the MiniTower mode frequencies (here as an example at 25 Hz). Similar PID filters are used for the SISO regulators for  $\theta_y$  and the  $y$  degree of freedom. All filters have a unity gain frequency at about 3 Hz and phase margins of more than 30 degrees.

The roll-off filter is a 1<sup>st</sup> order elliptic filter in combination with a 2<sup>nd</sup> order Butterworth filter at 30 Hz. The elliptic filter is used for a steep roll-off with minimal phase loss around the UGF. An additional benefit of the elliptic filter is that it features a notch, which can be aligned in frequency with the first rigid body mode of the MiniTower.

MultiSAS was installed in the MiniTower and, after mechanical installation, fitted with a 320 kg dummy mass instead of the bench. The actuation matrix  $\mathbf{D}$  was determined first, by using the iterative procedure described in Ref. [14], and then the operation in closed-loop was tested. Typical results are shown in Fig. 13. The ground spectrum is plotted and the microseismic peak is clearly visible between 100 and 500 mHz. At 10 Hz, the motion is below  $10^{-8}$  m/ $\sqrt{\text{Hz}}$  and at higher frequencies the usual  $1/f^2$  slope is observed.

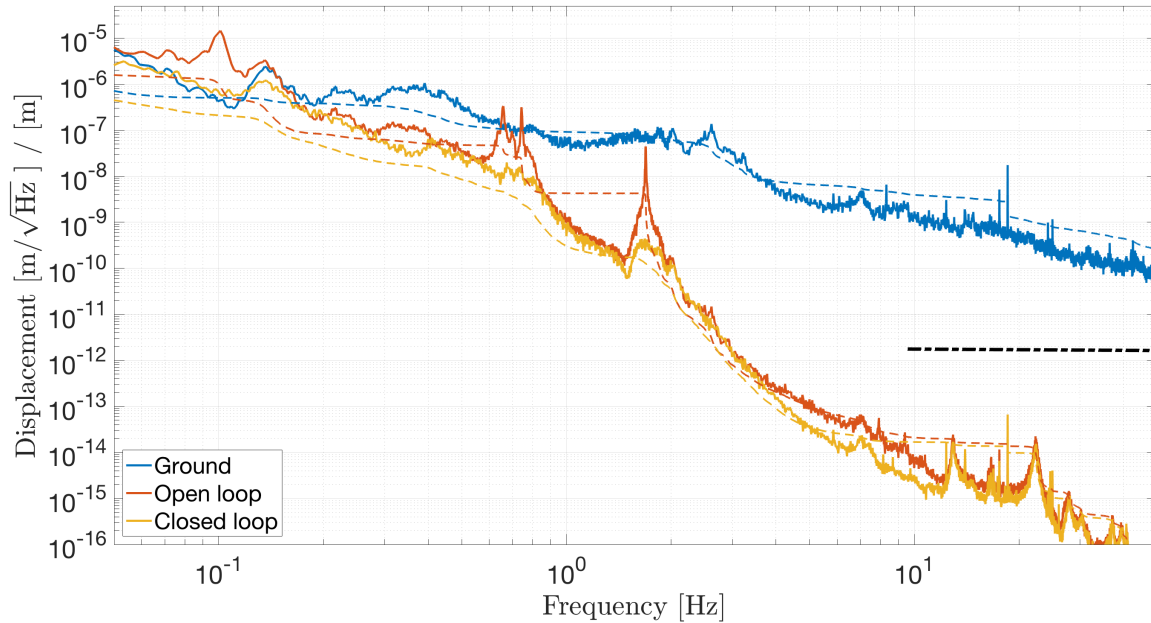


**Figure 13.** Estimated open and closed loop spectral (solid) and rms (dashed) results in the  $z$ -direction from MultiSAS loaded with a dummy mass. The measurement is performed by a witness out-of-loop L4C geophone placed on the suspension top stage. Below 50 mHz, geophone self noise dominates the result. The plot shows the expected bench motion reconstructed by multiplying the witness sensor signal by the measured top stage to bench transfer function. The translational spectral requirement from 10 Hz is shown as a black dashed line. Displacement levels better than  $10^{-14}$  m/ $\sqrt{\text{Hz}}$  are achieved above 10 Hz. At 12 and 22 Hz, the main modes of the tank are observed.

An out-of-loop witness geophone was placed on the top stage in order to measure the system performance. The signal of the witness geophone was also used to estimate the residual motion of the suspended bench. This is achieved by multiplying the witness sensor signal by the measured reconstructed top stage to bench transfer function. It must be noted that this projection gives a more realistic estimate of the residual bench motion since, unlike the MultiSAS transfer function in Fig. 5, it also includes the mechanical response of the Minitower to the ground motion.

In open loop, the MultiSAS modes at around 0.1 Hz (inverted pendulum stage), 0.7 Hz (common composite pendulum mode) and 1.8 Hz (differential composite pendulum mode) are observed. The attenuation slope increases to  $1/f^6$  above to last mode at 1.8 Hz. The official translational ASD requirement of  $2.1 \times 10^{-12}$  m/ $\sqrt{\text{Hz}}$  is surpassed by more than two orders of magnitude in the horizontal degree of freedom. When the rigid body modes of the suspension are effectively damped by the controls, the integrated rms displacement reduces to a fraction of a micron.

The MiniTower vacuum vessel modes should be monitored as this motion couples to angular motion. Also found in Fig. 13, the tank modes are clearly visible in the top stage motion and can end up as horizontal motion at the suspended bench level. This motion couples directly to pitch and roll and could spoil the angular performance as

shown in section 3. Further inspection of Fig. 13 reveals MiniTower modes above 10 Hz.

## 6. Conclusions and Future Work

The measurement of gravitational waves has been possible only because most (optical)  
315 elements of the detectors have been decoupled from the Earth's ever-present seismic  
motion. In the Advanced Virgo design, the decoupling is necessary for the core optics of  
the detector as well as the auxiliary optics. Some of these auxiliary optics are housed on  
optical benches, which are decoupled using vibration isolation systems. Five Multistage  
Seismic Attenuation Systems (MultiSAS) have been designed, constructed and tested  
320 by Nikhef and delivered to Advanced Virgo.

FEM and state space modeling have thought us about the (internal) mechanical  
modes of the system, designing and installing dampers where this was deemed  
necessary. Five more systems were constructed with the lessons learned from the  
first characterization campaign and, so far, the systems are behaving according to  
325 expectation, designed to meet requirements set by the Advanced Virgo design.

Thermal shielding has been designed and tested to prevent the GAS filter blades  
from sagging beyond displacements unrecoverable by the fishing rod devices. MultiSAS  
performance shows to be compliant with set requirements and no serious problems have  
been encountered. If the vacuum envelope of a MultiSAS is at 1 mbar pressure, then  
330 it has been tested to be enough not to have a measurable acoustic coupling. The  
construction tolerances have been such that the so-called cradle effect has no effect on  
the inertial sensors on the top stage used for control.

Already more systems are planned to suspend the squeezing optical table and  
(filtering) cavity mirrors for Advanced Virgo. The Australian National University  
335 (ANU) Centre for Gravitational Physics will use MultiSAS to suspend their low-  
frequency torsional pendulum TorPeDO [21]. Further advancement in advanced control  
strategies, such as was already done for the vertical degree of freedom with a dummy  
mass [22], will improve rms performance by better predicting the plant behavior upon  
actuation and using that information accordingly.

340 The test facility now serves as an advanced sensing and control test-bed at Nikhef.  
On the table, a monolithic accelerometer with an interferometric readout [23, 24] and a  
MEMS accelerometer [25] (both Nikhef projects) and Innoseis Tremornet<sup>TM</sup> sensors [26]  
are tested and characterized in a vibrationally quiet and vacuum environment.

## Acknowledgments

345 The authors would like to thank Michiel Jaspers, Willem Kuilman and Arnold Rietmeijer  
for constructing the MultiSAS prototype set-up and their hand-on experience in  
improving the design for the five Advanced Virgo systems. We would like to thank  
Marco Kraan for producing the artist impressions of the system. Lastly, Fred Schimmel  
has designed the LVDT actuator pairs for the bench control and has done lots of Labview

work. This work is (partly) financed by the Netherlands Organisation for Scientific  
 350 Research (NWO).

- [1] B.P. Abbot *et al.*, "Observation of Gravitational Waves from a Binary Black Hole Merger", Phys. Rev. Lett., vol. 116, pp 061102 (2016)
- 365 [2] F. Acernese *et al.*, "Advanced Virgo: a second-generation interferometric gravitational wave detector", Class. Quant. Grav. 32(2), pp 024001 (2014)
- [3] J. Aasi *et al.*, "Advanced LIGO", Class. Quant. Grav. 32(7), pp 074001 (2015)
- [4] B.P. Abbot *et al.*, "GW170814: A Three-Detector Observation of Gravitational Waves from a Binary Black Hole Coalescence", Phys. Rev. Lett., vol. 119, pp 141101 (2017)
- 360 [5] B.P. Abbot *et al.*, "GW170817: Observation of Gravitational Waves from a Binary Neutron Star Inspiral", Phys. Rev. Lett., vol. 119, pp 161101 (2017)
- [6] B.P. Abbot *et al.*, "Multi-messenger Observations of a Binary Neutron Star Merger", ApJL, 484(2), L12 (2017)
- [7] T. Accadia *et al.*, "Performance of the Virgo interferometer longitudinal control system during the second science run" Astroparticle Physics, 34, Issue 7, pp 521-527 (2011)
- 365 [8] M. Mantovani, "SBE suspension requirements for automatic alignment purposes", Technical report, EGO VIR-0101A-12 (2012)
- [9] T. Accadia *et al.*, "Noise from scattered light in Virgo's second science run data" Class. Quant. Grav. 27, pp 194011 (2010)
- 370 [10] D.J. Ottaway, P. Fritschel, and S.J. Waldman "Impact of upconverted scattered light on advanced interferometric gravitational wave detectors" Opt. Express, 20(8), pp 8329 - 8336 (2012)
- [11] The Virgo Collaboration, "Advanced Virgo technical design report", Technical report, Virgo note VIR-0128A-12 (2012)
- [12] H. Tariq *et al.*, "The linear variable differential transformer (LVDT) position sensor for gravitational wave interferometer low-frequency controls", NIM A, 489, pp 570-576 (2002)
- 375 [13] J. Peterson, "Observations and modeling of seismic background noise", U.S. Department of Interior Geological Survey (1993)
- [14] M.G. Beker, "Low-frequency sensitivity of next generation gravitational wave detectors", Ph.D. thesis, VU University Amsterdam (2013)
- 380 [15] G. Cella *et al.*, "Monolithic geometric anti-spring blades", Nucl. Instr. and Methods in Phys. A 540(2), pp 502 - 519 (2005)
- [16] S. Marka *et al.*, "Anatomy of TAMA SAS seismic attenuation system," Class. Quantum Grav., vol. 19, pp. 1605–1614 (2002)
- [17] T. Sekiguchi *et al.*, "MultiSAS inverted pendulum transfer function measurement for counterweight tuning", Technical report, Virgo note VIR-0587A-17 (2013)
- 385 [18] A. Bertolini *et al.*, "MultiSAS heat shielding test results", Technical Report, Virgo note VIR-0497A-14 (2014)
- [19] Applied Geomechanics, "756-Series Mid-Range Miniature Tilt Sensors", <http://www.techsys.be/pdf/755-75620100007d.pdf>
- 390 [20] J.V. van Heijningen, "Low-frequency performance improvement of seismic attenuation systems and vibration sensors for next generation gravitational wave detectors", Ph.D. thesis, VU University Amsterdam (2018)
- [21] D.J. McManus, P.W.F. Forsyth, M.J. Yap, R.L. Ward, D.A. Shaddock, D.E. McClelland and B.J.J. Slagmolen, "Mechanical characterisation of the TorPeDO: a low frequency gravitational force sensor", Class. Quant. Grav., vol. 34, 13, pp 135002 (2017)
- 395 [22] M.G. Beker *et al.*, "State observers and kalman filtering for high performance vibration isolation systems", Review of Scientific Instruments 85 (2014)
- [23] J.V. van Heijningen *et al.*, "Interferometric readout of a monolithic accelerometer, towards the fm/ $\sqrt{\text{Hz}}$  resolution", Nucl. Instr. and Methods in Phys. Research A 824, pp 665–669 (2016)
- 400 [24] J.V. van Heijningen *et al.*, "A novel interferometrically read out inertial sensor for future

gravitational wave detectors”, 2018 IEEE Sensor Application Symposium proceedings, pp 76-80 (2018)

[25] B.A. Boom *et al.*, ”Nano-g Accelerometer using geometric anti-springs”, 2017 IEEE 30th International Conference on Micro Electro Mechanical Systems (MEMS) proceedings, pp 33-36 (2017)

405

[26] Mark Beker *et al.*, ”Innovations in seismic sensors driven by the search for gravitational waves”, *The Leading Edge* 35(7), pp 590–593, <https://doi.org/10.1190/tle35070590.1> (2016)